

Effects of concentrated solar irradiation on allotropic transformations of AISI 316 stainless steel

Omar Álvarez^{a,✉}, Armando Rojas^b, Arturo Barba^c, Camilo A. Arancibia^a, Jorge Álvarez^d, Dulce V. Melo^e, Carlos E. Arreola^a

^aInstituto de Energías Renovables (IER). Universidad Nacional Autónoma de México (UNAM), Xochicalco, 62588 Temixco, Morelos, México

^bCentro de Ingeniería Avanzada, Dpto. de Termofluidos, Facultad de Ingeniería, Universidad Nacional Autónoma de México (UNAM), Ciudad Universitaria, 04510 México, CDMX

^cCentro de Ingeniería de Superficies y Acabados (CENISA). Facultad de Ingeniería. Universidad Nacional Autónoma de México (UNAM), Ciudad Universitaria, 04510 México, CDMX

^dDpto. de Ingeniería y Arquitectura. Instituto Tecnológico y de Estudios Superiores de Monterrey (ITESM) Campus Cuernavaca, Autopista del Sol km 104, Real del Puente, 62790 Xochitepec, Morelos, México

^eDpto. de Mecatrónica del Tecnológico de Monterrey. Instituto Tecnológico y de Estudios Superiores de Monterrey (ITESM) Campus Estado de México, Carretera Lago de Guadalupe km 3.5, Atizapán de Zaragoza, México, 52926, México

[✉]Corresponding author: omalb@ier.unam.mx

Submitted: 14 December 2017; Accepted: 13 June 2018; Available On-line: 19 October 2018

ABSTRACT: This study investigates the phase transformations that can occur in an austenitic stainless steel (AISI 316) by demonstrating the appearance of δ -ferrite that is obtained in the initial heating cycles using Concentrated Solar Irradiation (CSI) at magnitudes needed to obtain the operational temperatures of central tower systems. Four AISI 316 stainless steel specimens cut from one single initial piece, were exposed to CSI in the Horno Solar de Alto Flujo Radiativo at the Universidad Nacional Autónoma de México to perform the thermal cycles. AISI 316 stainless steel is fully austenitic and is selected because it is reportedly one of the cheaper material used in CSI receivers. Monotonic tensile strength tests were performed, and it is assumed that there is no relevant effect on the mechanical behavior for the reported experiment. Phase transformations were characterized using optical microscopy, X-ray diffraction and by scanning electron microscopy analysis with an energy-dispersive X-ray spectroscopy. The appearance of δ -ferrite phase was the principal difference between CSI treated specimens, a non-treated specimen and one specimen heated by conventional method. Concentrated UV irradiation from the solar spectrum on Earth surface demonstrated to have the potential to obtain the phase transformation at a temperature near 630 °C.

KEYWORDS: Austenitic; Allotropic transformations; Concentrated solar irradiation; Stainless steels; δ -ferrite obtained

Citation/Citar como: Álvarez, O.; Rojas, A.; Barba, A.; Arancibia, C.A.; Álvarez, J.; Melo, D.V.; Arreola, C.E. (2018). "Effects of concentrated solar irradiation on allotropic transformations of AISI 316 stainless steel". *Rev. Metal.* 54(4): e133. <https://doi.org/10.3989/revmetalm.133>

RESUMEN: *Efectos de la irradiación solar concentrada en las transformaciones alotrópicas del acero inoxidable AISI 316.* Se investiga la transformación de fases que pueden ocurrir en un acero austenítico (AISI 316) mediante la demostración de la aparición de ferrita- δ que se obtiene en ciclos iniciales de calentamiento usando irradiación solar concentrada (ISC) a magnitudes necesitadas para obtener temperaturas de operación de sistemas de tipo torre central. Cuatro especímenes de acero inoxidable AISI 316 cortados de una misma pieza, fueron expuestos a ISC en el Horno Solar de Alto Flujo Radiativo de la Universidad Nacional Autónoma de México para desarrollar el ciclado térmico. El acero AISI 316 fue seleccionado por ser reportado entre los materiales más baratos usado en receptores de ISC. Pruebas de resistencia a la tensión monotónica demostraron que no existe un efecto relevante del ciclado térmico en las propiedades mecánicas resultantes. Las transformaciones de fase fueron caracterizadas usando microscopía óptica, difracción de rayos X, y microscopía electrónica de barrido con espectroscopía de dispersión de energía de rayos X. La aparición de la fase de ferrita- δ fue la principal diferencia entre los especímenes tratados con ISC y dos especímenes de referencia. La fracción UV de la ISC demostró tener el potencial de lograr estas transformaciones de fase a una temperatura cercana a los 630 °C.

PALABRAS CLAVE: Acero inoxidable; Austenítico; Ferrita- δ obtenida; Irradiación solar concentrada; Transformaciones alotrópicas

ORCID ID: Omar Álvarez (<https://orcid.org/0000-0002-2414-2471>); Armando Rojas (<https://orcid.org/0000-0003-4989-9371>); Arturo Barba (<https://orcid.org/0000-0001-7285-9429>); Camilo A. Arancibia (<https://orcid.org/0000-0001-6782-0116>); Jorge Álvarez (<https://orcid.org/0000-0001-5105-2677>); Dulce V. Melo (<https://orcid.org/0000-0001-7488-7677>); Carlos E. Arreola (<https://orcid.org/0000-0003-4770-8340>)

Copyright: © 2018 CSIC. This is an open-access article distributed under the terms of the Creative Commons Attribution 4.0 International (CC BY 4.0) License.

1. INTRODUCTION

There have been several advances in the development of technologies oriented towards using CSI as an energy source because it is a free source of energy. However, with these advances, there are also new challenges to improve the operational lifetime of the devices and installations to compete with conventional technologies and reduce the pollution problems that are linked to the use of fossil fuels. Therefore, for CSI technologies, the absorber materials must withstand the demanding conditions of the normal operation of the systems, which are associated with the damage in metallic alloys, intermittence of the energy resource and combined phenomena at high temperatures, such as corrosion and an uneven CSI distribution across the absorber. Moreover, the challenge to lower the installation and maintenance costs remains.

These efforts attempt to answer the questions regarding the useful lifetime of a material when it is exposed to CSI in the cyclic critical conditions of high temperatures, as observed in the investigations of Rojas-Morín and Fernández-Reche (2011), such as the magnitude of the concentrated solar fluxes, the thermal and mechanical stresses that develop during operation and the degradation of mechanical properties.

The challenges involve maintaining the operation of solar energy concentration systems with a higher efficiency and longer operation lifetime and overcoming the problems related to the CSI, i.e., corrosion and intermittence of the resource.

As widely discussed by Augsburger and Favrat (2013), additional factors, such as the permanent degradation of materials in solar central tower receivers and the appearance of clouds, which enables the occurrence of thermal cycles, contribute to the solar thermal fatigue phenomena. Fatigue and thermal fatigue result in the appearance of cracks due to cyclic thermal stresses, which degrades the mechanical properties of the materials, as determined by Klobčar *et al.* (2008), and can cause failure of the elements, even at magnitudes of stresses that are lower than the yield strength (Fine and Chung, 1996).

The expected answers from investigating the materials exposed to CSI will provide valuable information to improve component design, allow the higher possible temperature by receiving the highest magnitude of heat flux, give guidance on managing the operation of solar power towers, understand the reasons for degradation and their effects on the performance of the materials and provide an overview for further investigations on the solar thermal transformations in metallic materials. To determine the effects on the materials and elements used in central tower receivers, these experiments must reproduce both normal and extreme operating conditions

based on the geometry of the elements used in the solar receivers for central towers and the combined effects of high speed cycles, oxidation, and possible transformations in metallic alloys that could lower mechanical performance and corrosion resistance. As demonstrated by Boubault *et al.* (2012) and Boubault *et al.* (2014), the radiative properties are affected by aging, which is caused by the exposure of the materials to continuous or cyclic CSI.

The objective of this study is to determine the phase transformations in AISI 316 stainless steel and evaluate the modifications in its mechanical properties under tension with a traction test, associated to CSI. Prasad and Kumar (2013) used induction heating to study thermo-mechanical fatigue and adjust the thermal gradients to normalized data; however, this theoretical method does not reproduce the conditions of the incident solar spectrum in CSI systems. Zhang *et al.* (2013) studied the efficiency of an experimental receiver heated by an electric Joule effect; however, it should be noted that their study does not include the incidence of the CSI spectrum or even the thermal gradients caused by the flux distribution. Therefore, the materials will not be affected by the components of the solar spectrum (the infrared, visible and UV components) as when subjected to the CSI, which have proven benefits including an allotropic transformation activation effect, as noted by Herranz and Rodríguez (2010), and enables the design of materials based on the absorptivity in the UV regime, but this would presumably have a negative effect on the lifetime of the materials of solar receivers providing sensitivity to mechanical loads and corrosion. Although Rodríguez-Sánchez *et al.* (2014) demonstrated that the thermal stresses are lower than the ultimate tensile strength and will not fracture the components, other negative implications may be present. Thus, we observe a mechanism that we denote as solar thermal degrading effects.

A performed analysis (Boubault *et al.*, 2012) of different factors that result in aging on Inconel 625 flat plates, which were covered with Pyromak 2500; however, it is also necessary to use the accurate cylindrical geometry of the tubular pipes in the receivers and provide an overview of the behavior of the materials if Pyromak 2500 degrades to elimination. Boubault *et al.* (2014) presented results on flat plates, in which aging causes a reduced performance of the thermal radiative, heat conductivity, and mechanical properties; in particular, the reduction in the heat conductivity properties results in higher thermal gradients, responsible for the development of higher stresses and mechanical fatigue.

In this study, several cylindrical and tubular pieces (referred to, henceforth, as specimens) with similar dimensions to those used in solar central receivers were used to perform an aging and damage experiment in the Horno Solar de Alto Flujo

Radiativo (HoSIER) of the Universidad Nacional Autónoma de México in the Instituto de Energías Renovables. These experiments were performed using AISI 316 stainless steel, which is one of the materials used in the solar central receiver because of its corrosion resistance at elevated temperatures and its good mechanical resistance.

The thermal conditions of the cyclic experiments were selected based on the high and low temperatures of molten salt in the central solar receivers of 565 °C and 285 °C, respectively; the conditions were set at the back of the cylindrical tubular specimen to approach the molten salt heating conditions and similar temperatures of receivers that operate with gases, as reported in (Boerema *et al.*, 2012; Rodríguez-Sánchez *et al.*, 2014).

The experiments determined that the first 35 to 90 solar thermal cycles with the hot and cold salt temperatures, which are typically used for this type of concentrating solar system, have no impact on the mechanical properties of the tensile strength resistance but result in a transformation of the metallic matrix. These thermal cycles are caused not only by cloud passages with a transient characteristic but also by the normal operation of this type of power plant during natural nighttime periods (Augsburger and Fravat, 2013; Ho and Iverson, 2014).

Jianfeng *et al.* (2010) developed a model in which the angular variation of absorptivity over the circular surface of a cylindrical pipe is considered. They explained that different effects are inevitable because the thermal gradients are caused by the angular influence; in addition, due to the optical configuration of solar concentrated systems, the material elements will be affected by both the section that receives radiation and the section that does not receive radiation. The results of Rodríguez-Sánchez *et al.* (2014) agreed with this statement, and argue that the thermal losses have to be also considered in the model.

A monotonic traction test was performed to determine a different behavior in mechanical properties

in this sense; and a X-ray diffraction test were performed to determine the transformations of the metallic matrix. We found that the first thermal cycles performed using CSI have a remarkable influence on the transformation of the initial metallic phase of AISI 316 SS, which occurs due to the UV spectrum. Therefore, we determine a strong influence of the UV radiation portion of the solar spectrum. We observe that the UV component in the solar spectrum, unlike the visible or infrared components, is able to generate a crystalline phase, which is identified as δ -ferrite and that the amount of the developed phase does not increase yield and tensile strength significantly shown in results.

Because it is not possible to study specimens over the course of their extended service lifetimes, an accelerated-cycle CSI experiment is proposed based on the operation of the afore mentioned systems; this experimental method is proposed to analyze the phase transformations, as described by Boubault *et al.* (2014) in tubular receivers with liquid or gas heat transfer fluids and to improve the understanding of the material transformation by allotropic phenomena. Thus, the transformation of the stainless steel is confirmed when a crystalline phase, which is strongly related to the fraction of the UV component of the solar spectrum, is obtained.

2. MATERIALS AND METODS

2.1. Description of the facility

The HoSIER is a solar furnace located at the Laboratorio Nacional de Sistemas de Concentración y Química Solar in the Universidad Nacional Autónoma de México, and it is a horizontal axis furnace with a focal point located 3.68 m from the faceted concentrator mirror. This facility is best described by Riveros-Rosas *et al.* (2010).

As shown in Fig. 1, the specimens were placed in a specimen holder designed for the HoSIER, whose

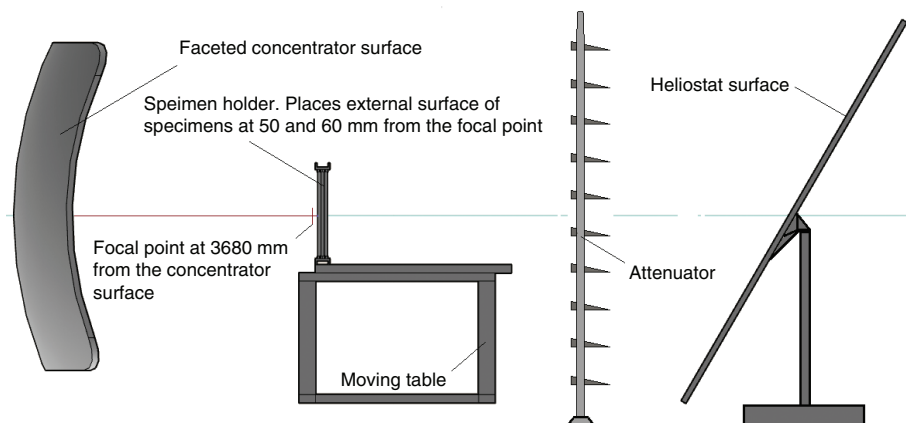


FIGURE 1. Schematic of the experimental facility, as illustrated by the authors.

dimensions ensure that the specimens are irradiated with a concentrated solar flux. This holder was placed over the moving table and had inlet and outlet holes for the cooling air flow; the specimens were placed 50 mm and 60 mm behind the focal point in the focal axis of the HoSIER. Furthermore, the holder was designed to experience negligible strain during the thermal expansion of the specimens.

2.2. Material selected for the experimental procedure

The material selected for the experimental procedure is the stainless steel AISI 316 because it is used in the receivers of central tower solar concentration systems. Other materials are used in this same application, such as nickel alloys known as Inconel or Incolloy; however, AISI 316 stainless steel is proposed because of its lower price and easy to get, compared with other materials. Stainless steels and nickel alloys are used as the material elements of the pipes and the structural elements in concentrated solar energy receivers because of their chemical resistance to corrosion and good mechanical behavior. Corrosion resistance is a significant property because the receiver is subjected to demanding conditions. For example, temperatures that approach 630 °C cause an increase in the temperature of the working heat transfer fluid, and these results in chemical instability of the typically used fluids, nitride salt and Hitec salt. Hence, the environmental, operative and high-temperature conditions demand good mechanical and chemical properties of the materials.

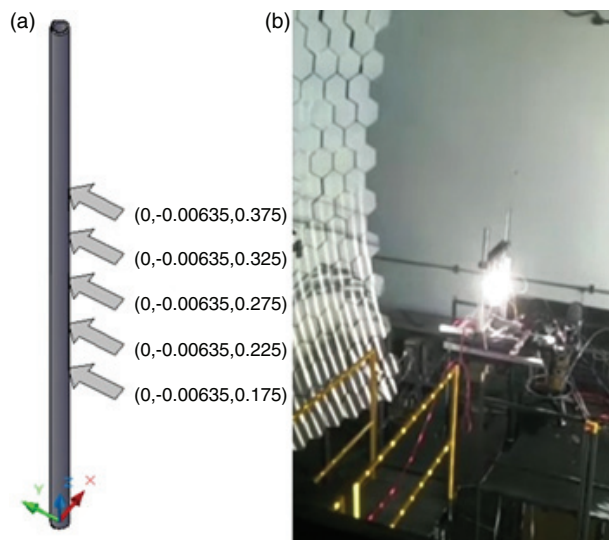


FIGURE 2. a) Specimen geometry with an external and internal diameter of 12.7 mm and 9.5 mm respectively, and a length of 550 mm; the locations of the thermocouples are indicated by arrows, and b) Exposure of a specimen during the warming stage of the thermal cycle.

Rodríguez-Sánchez *et al.* (2014) and Ho and Iverson (2014) have emphasized that the diameter of the tube of the receiver must be controlled, as it affects the heat transfer efficiency and pressure losses. The determined geometry of the cylindrical tubes should be close to an external and internal diameter of 12.7 mm and 9.5 mm, respectively; to provide an equilibrium between both aspects of heat transfer efficiency and pressure losses. As indicated in Fig. 2a, this is the selected geometry for the specimens, with a length of 550 mm. The tubes are typically radiated by the concentrated solar flux from the heliostat field.

The denomination of the austenitic stainless steel AISI 316 is ASTM A 313, and it has a nominal composition of Cr 16%–18%, Ni 10%–14%, and Mo 2%–3%. It is well known that the carbon content is approximately 0.08%, and the remaining mass percentage is composed of Fe. AISI 316 is a widely used material for applications that require good heat resistance and a larger corrosion resistance than that of austenitic stainless steel AISI 304.

Sibin *et al.* (2015) reported an absorptivity of solar radiation of 0.3835 for stainless steel and an emissivity of 0.125, both of which are considered as average values. These values are used to develop a heat transfer model, prior to experimentation.

2.3. Thermal cycles obtained by the CSI

The specimens were radiated by exposure to a concentrated heat flux from the faceted concentrator in the HoSIER. The flux was used to achieve the required temperatures, and the shape of this flux was described in a previous study by the authors.

Two specimens were placed at each distance to obtain a couple of specimens with each solar flux distribution. Because the specimens are placed at both distances, the concentrated solar flux for the specimens located at 60 mm covers a larger length but exhibits a lower power density. Thus, it is necessary to open the attenuator between the faceted concentrator and the heliostat to obtain the required temperature for the specimens at a longer distance from the focal point in a similar amount of time. In a previous study by the authors, it was demonstrated that the temperature profile in the rear zone (considered as the zone with no direct exposition to the concentrated solar flux) of the specimens reaches the required temperature in the time obtained by a simulation performed using COMSOL MULTIPHYSICS® modeling software. Additionally, because the radiative properties of stainless steel, in the presence of oxides besides the initial chromium oxide, are not known, the thermo-radiative properties cannot be implemented in the simulation, and it is not possible to determine the amount of time in which the temperature approaches the operational temperature of the receivers; thus,

only the amount of time in which the temperature profile reached a temperature of 200 °C or 250 °C can be obtained. Furthermore, it is only possible to confirm that the experiment approaches the temperature of the pipes in the receiver because at higher temperatures, the surface of the specimens contains oxides beside the initial chromium oxide.

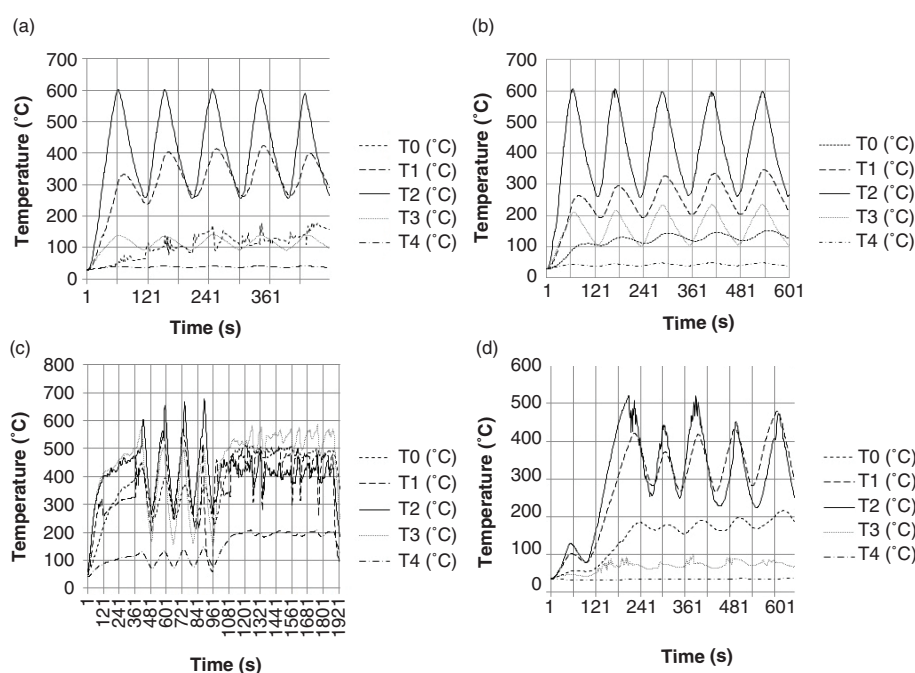
Once the specimens were placed at distances of 50 mm and 60 mm behind the focal point of the HoSIER, air-flow was channeled through the interior of the tubular cylindrical specimens at $8 \text{ m}^3 \text{ hr}^{-1}$ (representing a bulk velocity of 31.35 m s^{-1}) to maintain the removal of heat energy from the specimen material. The attenuator was automatically controlled with a program developed by the authors in LabView® by National Instruments® to allow irradiation through the concentrator of the HoSIER until the temperature of “hot salt” at 565 °C was recorded for the specimens by any of the thermocouples. Subsequently, the attenuator was closed to enable cooling by internal forces and external natural convection to the temperature of “cold salt” at 285 °C. These temperatures were reported by Boerema *et al.* (2012) as the typical operation temperatures for central tower solar concentration systems. Fig. 2b shows one of the specimens during the warming up process.

2.4. Experimental procedure

There is a mobile table inside the HoSIER that is controlled to adjust the specimen position, and it can be moved during the experiment.

In the experiment, the specimens are located at two fixed distances of 50 and 60 mm from the focal point. Two programs were implemented to ensure the accurate execution of the experiment. One of the programs was written to open and close the attenuator of the HoSIER. Once the maximum temperature of 565 °C in the specimens was reached and the attenuator was opened at a percentage from 20% to 40%, the program detected the temperature using a K-type thermocouple. Then, the program was executed to close the attenuator until the lower temperature of 285 °C was reached. Lastly, the program reopened the attenuator to begin a new cycle. The thermal history of each specimen for the first five cycles is illustrated in fig. 3. Because each thermocouple was placed at the rear section of the specimens, it is assumed that this represented the thermal condition to ensure that the heat transfer working fluid reached the highest operation temperature after warming up. Then the attenuator was closed, as if a dense cloudy condition would happen until the fluid reached the lower temperature slightly before the salt inside the pipes froze.

In Fig. 3 (a-c) it is observed that the specimens suddenly reach a higher temperature of 600 °C and a lower temperature of 270 °C in the central zone of the geometry (which is where the control command of the attenuator is assigned). These phenomena occur because of the combination of physical conditions known as “thermal inertia”, which occurs when the attenuator does not close



or open immediately due to the operation of the mechanical system, and the surrounding air causes continuous cooling.

Table 1 presents the thermal aspects of the behavior of each experiment for each specimen. As observed here and similar to what typically occurs in real systems, the time the experiment lasts cannot be the same because, at that specific moment, there could be a cloud passing, which reduced the irradiation in Temixco, Morelos, México.

3. RESULTS AND DISCUSSION

3.1. Mechanical monotonic tensile test

It is reported that the mechanical integrity of the elements in solar energy receivers must be considered because mechanical elements may suddenly fail due to the degradation of the mechanical properties, which results from photo-thermal fatigue and the oxidation and corrosion that lead to the eventual chemical decomposition of the heat transfer fluid.

In this experiment, the chemical decomposition of a heat transfer fluid is avoided because the irradiated specimens are cooled by air; however, other degrading factors remain. Thus, the effect of mechanical degradation in the first 40 to 90 cycles on the geometry of the stainless steel should be evaluated.

Because the magnitude of ultimate strength can be affected—which would reveal if there is degradation in this mechanical property—the mechanical analysis for each specimen is reported and compared with that for the specimen with no exposure to the concentrated solar irradiation. The equipment used to perform the evaluations was an Instron® universal machine, Mod. 1125, with a maximum load capacity of 100 kN. The software used to register the tension loads was Series IX 8.30.00 with an interface Instron 5500®. Figure 4 depicts the mechanical behavior in the monotonic tensile test.

The mechanical behavior in the monotonic tensile test at a strain rate of 1.5 mm min^{-1} for specimens A, B, C, and D and the specimen with no exposure to CSI, and there is no substantial change in the mechanical properties to tensile test; thus, it can be assumed that for the initial photo-thermal cycles, the mechanical properties are not affected by apparent changes.

Due to the distribution of the concentrated solar energy and because it is affected by the slope error and other optical influences, there is always a concentrated solar flux with a particular distribution of the irradiance that reaches the receiver. Gradients in the concentrated irradiance will result in gradients in the thermal field of the receiver, which will lead to thermal stresses. The thermal fatigue is caused by the cyclic appearance of thermal stresses,

TABLE 1. Thermal aspects of the behavior for each experiment. The maximum temperature is registered in the thermocouple located at (0, -0.00635, 0.275), which can be observed in Fig. 2a.

Specimen	Distance from focal point	Total number of cycles	Total experiment time (s)	Max temp. (°C)
A	50 MM	91	6 000	603.72
B	50 MM	89	12 700	660.90
C	60 MM	38	3 100	676.99
D	60 MM	67	6 500	583.51

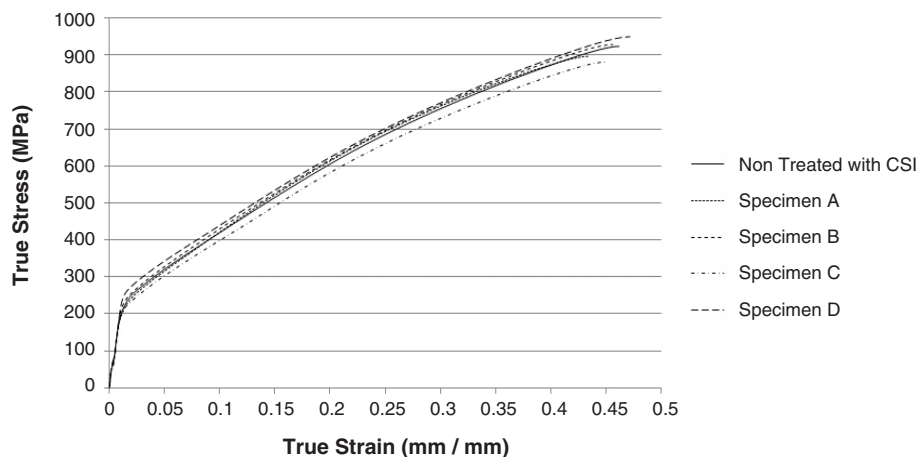


FIGURE 4. True stress-true strain curves for each specimen.

and it is possible to assume that this thermal effects performed by solar concentration will enhance the degradation also by the incident solar spectrum; however, this is negligible for at least the first 90 photo-thermal cycles regardless of the distribution of concentrated solar heat flux and the overheating of the specimen.

$$\sigma = \sigma_0 + K\varepsilon^n \quad (1)$$

Table 2 lists the strain-hardening exponent n and the strength coefficient K of the stainless steel for each specimen. The value of σ_0 is also provided, which is necessary to “cut” data and determine where the flow curve begins. The Ludwik equation (Eq. 1) for each of the specimens indicates no substantial difference in their mechanical behavior, and any slight difference between them may be considered as experimental error.

TABLE 2. Parameters of the Ludwik (Eq. 1) developed for each of the specimens. σ_0 was found using the yield strength criterion; thus, the Hollomon region was recognized and the K and n coefficient and the exponent were obtained from the “flow curve”, as specified by Dieter (2000).

Specimen	σ_0	K	(n)
Non treated with CSI	216.00	1927.35	0.4429
A	212.92	1988.23	0.4535
B	234.46	1948.47	0.4403
C	213.03	1887.10	0.4508
D	253.37	1876.75	0.4205

Lastly, it is proven that there is no relevant modification to the tensile mechanical properties for the photo-thermal cycles applied to the specimens.

3.2. SEM and EDXS analysis

For every specimen a scanning electron microscopy analysis (SEM) and an energy-dispersive X-ray spectroscopy (EDS) were performed to explore the composition, microstructure and phases present in the AISI 316 SS specimens before and after the experiment, using a Philips XL 20 scanning electron microscope. The objective was to compare any visible phase transformation between the non-treated specimen, the heated by conventional method and every specimen that underwent cyclic CSI exposition. Figure 5 show the SEM images starting with non-treatment specimen, the heated by conventional method and specimens A, B, C, and D respectively. This figures are also denoted by (a) and (b), for two different magnifications (100 and 800 X respectively). A punctual EDXS analysis was performed to obtain the elements in the composition over visible surface changes for every specimen. As no substantial difference over the non-treated was observed, no punctual EDXS analysis was performed. A black mark on (b) images show the point where the punctual EDXS was performed; this analysis revealed a predominant content of Fe and Cr only for CSI exposed specimens.

Figure 6 shows the atomic percentage of Cr, Fe, O, Ni versus maximum temperature in thermal cycle over the surface for every specimen. This figure was

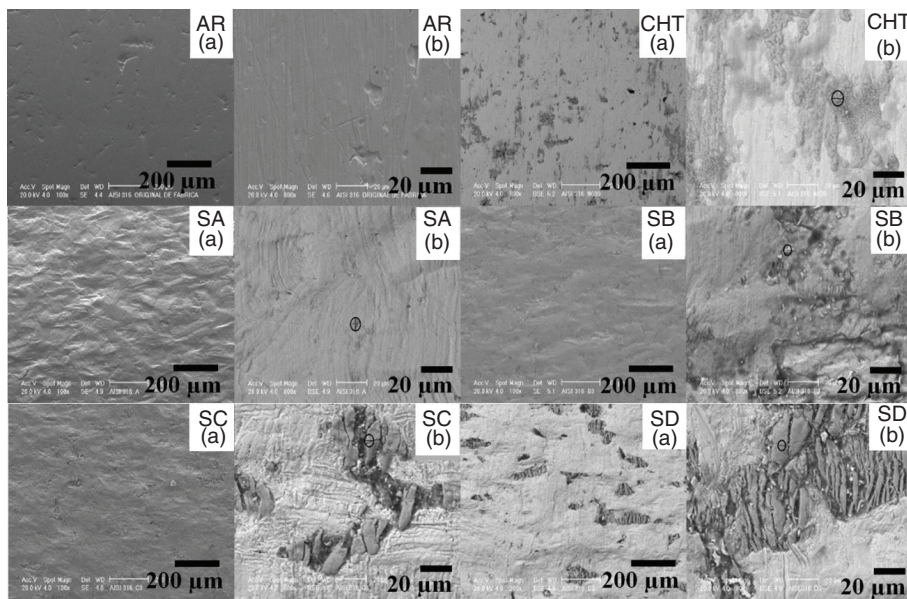


FIGURE 5. SEM images of (AR) non-treatment AISI 316 SS specimen, (CHT) conventionally treated AISI 316 SS specimen, (SA) specimen A, (SB) specimen B, (SC) specimen C, (SD) specimen D.

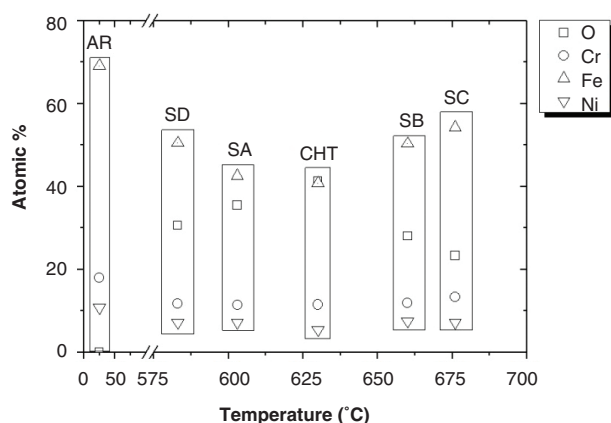


FIGURE 6. Change in Atomic % of Cr, Fe, O, Ni versus maximum temperature in thermal cycle.

elaborated based on EDXS analysis over the general surface for every specimen.

It is evident the single phase shown by the non-treatment specimen in Fig. 5 (AR). Fig. 6 (AR) then shows the non-affected atomic percentage of elements in AISI 316 SS.

A surface change is shown over the surface in the conventional method heated specimen in Figs. 5 (CHT (a-b)) revealing a oxygen content in the punctual EDXS analysis, it is then concluded a simple oxidation and Fig. 6 (CHT) confirms the highest atomic percentage of oxygen. The CHT was done also to have an approximated mean temperature to make comparisons; this CHT that lasted for 20 min at 630 °C was performed to obtain a uniform temperature using an Lindberg brand 1100 °C electric muffle furnace, and with a lineal heating and cooling rate of 0.5 °C min⁻¹ and -0.5 °C min⁻¹, respectively. The whole heat treatment with performed with the electric muffle furnace lasted for one hour.

Based on Fig. 6 for all specimens exposed to CSI, a higher Fe content on the surface with respect to the CHT specimen is noticeable; at the same time it is also shown that at higher temperatures the specimens are not likely to undergo further oxidation.

Since Cr and Ni superficial atomic percentage do not change for the CSI-treated specimens or for the CHT specimen, but the punctual EDXS analysis reveals a higher Cr content and lower Ni in the dispersed visible phases for CSI exposed specimens, it is possible to conclude the following. As Ni is used to retain the austenite in 300 series stainless steels, there is a phase change in the zones, where only Fe, Cr, and some Mn is found. Thus, the CSI exposed specimens experimented a phase transformation characterized by zones with an enrichment of Cr, and depleted Ni as it is described by Hsieh *et al.* (2008). All these aspects provide the possibility of δ -ferrite in the dispersed phases.

3.3. X-ray diffraction technique

To reveal the presence of other phases in the material, a comparison can be made between the specimens exposed to CSI in the HoSIER, the specimen with no treatment and the specimen that underwent conventional heat treatments. The equipment used was a Rigaku® DMAX 2200 X-ray diffractometer with Cu_{K α} radiation. All diffraction angles were compared to the database of the Joint Committee for Powder Diffraction Standards (JCPDS) to identify the phases; JCPDS 330397-316 SS, JCPDS FeCr 340396, JCPDS 330664- Fe₂O₃.

With the X-ray diffraction technique, there is an evident singularity present in each specimen treated by the CSI in Fig. 8 then compared to Fig. 7: at an angle of 44.8° where the X-ray diffraction peak is observed for conventional AISI 316 stainless steel, a developed phase is present, which is best identified by the software of the Rigaku® DMAX 2200 X-ray diffractometer to contain Fe and Cr (Yajiang *et al.*, 2002); the developed phase is also found to be present in other of these specimens with a X-ray diffraction peak at 65.2°. The developed δ -ferrite phase in the original matrix of AISI 316 SS is obtained in each exposed specimen due to the photo-thermal cycles performed, and it can be stated that the UV fraction in the CSI has a noticeable influence in its formation. The specimen with no heat treatment and the specimen heat-treated by conventional methods do not exhibit this phase; even, Sokolov *et al.* (2009), found in their calcination process at 500 °C that no new phases could be obtained in the original phases for their very similar austenitic alloy. Furthermore, it can be concluded that compared with specimens B, C and D, there is a secondary reflection peak as it is

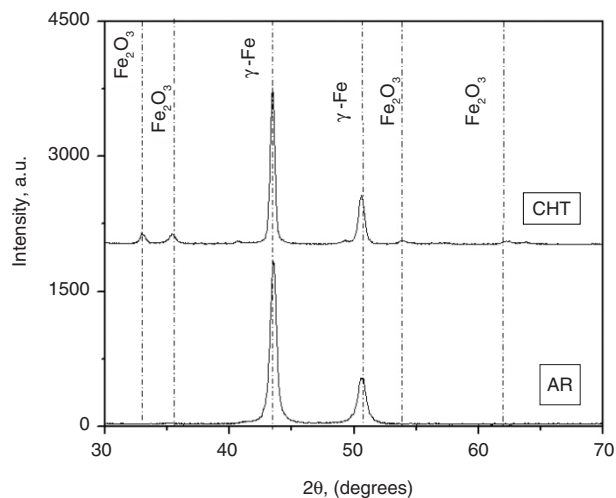


FIGURE 7. Diffractograms for specimens AR and CHT of AISI 316.

shown in the XRD pattern of Saeidi *et al.* (2015) just at the right of the common austenitic reflection peak of AISI 316 SS (γ -Fe), the formation of the δ -ferrite is obtained due to the CSI cycle experiment. For specimen A, there is no secondary reflection peak, but the initial formation of a peak is evident, that explains why in Fig. 6, there is the lowest Fe content in the specimen surface, considering all CSI exposed specimens. For specimens B and D, the “second peak” of the δ -ferrite phase is formed, even, these specimens have a similar content of Fe in the surface, and the characteristic peaks in Fig. 8 have also similar magnitude. Lastly, for specimen C, the formation of the δ -ferrite phase indicates a quantity that is present in higher proportions compared to the original phase and typical phases present in AISI 316 SS (γ -Fe); Fig. 6 show the highest contentment of Fe in the surface if compared with SA, SB, SD specimens. For each specimen, analysis was performed with both a penetrating X ray beam (2θ) and a beam at an angle of 0.5° (grazing incidence), with a speed analysis of 2° per minute, starting at 5° and ending at 78° ; however, as the same result was obtained for each specimen, only the 2θ results are presented. The only difference between a grazing-incidence and penetrating beam is that for the penetrating beam, the magnitude of every peak is lower due to the absorptive properties of the material in the X ray spectrum. Penetrating beam analysis was performed as 2 theta/theta mode starting at 5° and ending at 100° , also with a speed analysis of 2° per minute. From the diffractogram of the specimen without heat treatment depicted in Fig. 7, there is a single peak at an angle of approximately 43.78° , which is identified by the software as the typical composition of the crystalline structure of AISI 316 stainless steel (γ -Fe), similar to the remaining peaks observed. This first diffractogram

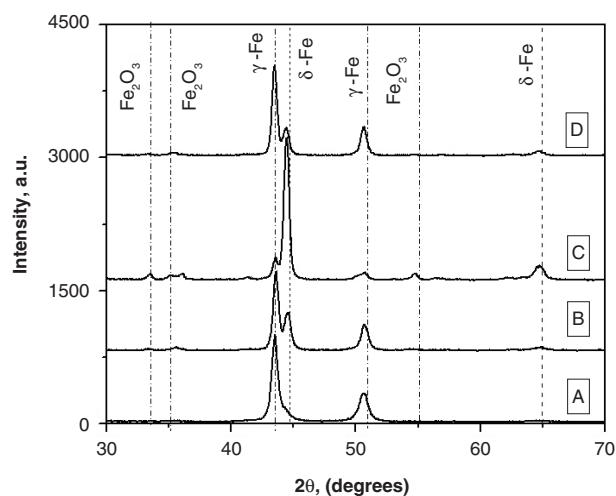


FIGURE 8. Diffractograms for specimens A, B, C and D of AISI 316.

corresponds to the same section (portion of the material) to which the treated specimens will be compared. The second case shown in Fig. 7 corresponds to the diffractogram of the CHT. This specimen was prepared to obtain a material with a heat treatment identified as conventionally heated at the same temperatures as those exposed in the HoSIER when the component was overheated. Furthermore, a single peak can be observed in the AISI 316 SS as austenitic phase shown by Saeidi *et al.* (2015); hence, it is confirmed that the temperature or the infrared radiation did not result in crystalline transformations stabilized at environment temperature in the material.

The findings of Brooks *et al.* (1991); Hsieh *et al.* (2008) and Padilha *et al.* (2013) have shown the formation of δ -ferrite, particularly in various processes of arc welding, laser welding and fusion molding; linked to the phenomena of solidification at generally high speeds, which cause the formation of dendrites. In this research, although fusion conditions are not reached, it is considered that solar radiation can cause diffusion processes of sufficient magnitude to generate the formation of δ -ferrite, as shown in the diffractograms of the treated specimens, which does not occur with the CHT specimen. It is shown in the ternary diagrams of Bechtoldt and Vacher (1957) that in the temperature up to 815.5°C for Fe-Ni-Cr-Mo system, δ -ferrite is not a noticeable phase component of the solid solution for AISI 316 stainless steel. Hence, it can be stated that a possible explanation for the appearance of δ -ferrite is the action of solar irradiation and -in particular- of the UV component, which is the component that is not presented in conventional heating in the electric muffle furnace. Furthermore, Vacher and Bechtoldt (1954) found a tendency of their investigated steels to nucleate δ -ferrite in the existing δ sites, and stated that the formation of δ -ferrite was continued by diffusion; therefore, we suggest that new δ -ferrite could be initiated in the surface where the UV radiation has incidence, but later continued by diffusion as found in the following description. Other phenomena with the characteristic enhancement, can be associated with the research of Herranz and Rodríguez (2010), in which it is explained that the use of solar radiation has allowed in various processes such as nitriding with salts, sintering of metal powders, and even in manufacturing ceramic components; process times and temperatures significantly reduced because of an observed phenomena denominated *photoactivation*. This can also be explained by the presence of this component of solar radiation. El Nayar and Beech (1986) argue that δ -ferrite can be formed from solid solutions of high or low $CrEq/NiEq$ ratios, since the transformation of this phase can be achieved depending on the cooling rate; in the case of our research, different cooling and

heating rates were obtained in the cycles of exposure to the CSI; however Padilha *et al.* (2013) concludes that the appearance of δ phase is more influenced by the composition of the solid solution than to the cooling velocity. According to Schaeffler diagram and the expressions presented by El Noyal and Beech (1986), the calculated $CrEq/NiEq$ is ~ 1.44 , which is considered a low ratio according to the same authors, and there is an initial amount of 5% δ -ferrite.

For specimen A, there is a noticeable difference; the initial formation of a new peak is observed to the right side of the first austenitic peak. This new formation, which is still not a new peak but represents the formation of a new peak, is identified as δ -ferrite. It corresponds to a developed phase with crystalline characteristics, but it does not modify the mechanical properties in the tensile test of the specimen as it is previously described.

For the diffractogram of specimen B, there is formation of a “second peak” at the right side of the austenite peak. For these peaks, the software reports a “crystalline mineral”, which is a phase identified as δ -ferrite, with an orientation of Miller index of (110); this indicates the formation of this new crystalline phase in the matrix of the material. A notable characteristic can be found by comparing specimens A and B in Fig. 8: this developed crystalline phase is formed, and it begins to grow. For the untreated specimen and the specimen with a conventional heat treatment, this peak is not present. For the diffractogram of specimen C in Fig. 8, the formation of the new crystalline phase reveals a peak that is even greater in intensity than the peak of the original austenitic phase in the AISI 316 SS (γ -Fe). This characteristic indicates that the UV portion of the solar spectrum leads to the generation of the developed δ -ferrite phase. This developed phase is identified as to be composed of Fe and Cr elements.

Lastly, for the diffractogram of specimen D in Fig. 8, the formation of the secondary peak at the right of the austenitic phase is observed. The formation of the δ -ferrite crystalline phase occurs for each specimen with the cyclic CSI treatment; however, it does not occur for the specimen with the conventional heat treatment at the temperatures experimented.

3.4. OM analysis

This micrographs are obtained using an Olympus® GX51 microscope. The images were obtained for the surface of an area cut perpendicular to the longitudinal axes of the cylindrical geometry, which were treated with sand paper and polished with saturated alumina solution of $0.3 \mu\text{m}$ grain size. Optical microscopy analysis was performed for each one on the specimens with two etchants. The

first was a mixture of hydrochloric acid (HCl), nitric acid (HNO_3) and acetic acid ($\text{CH}_3\text{-COOH}$), with performed immersion of 15 to 20 s, and it is denoted as etchant 1. Etchant 1 was used to reveal austenitic characteristics; as after the mechanical traction test there was no noticeable difference between all specimens, only Fig. 9 is shown, exposing that austenite is the primary crystalline structure.

The second OM analysis was performed using a mixture of saturated hydrochloric acid (HCl) and ferric chloride (FeCl_3), denoted as etchant 2. This etchant is reported by Vander Voort (1999) to be coloring agent for δ -ferrite, and it is used to prove the increase of this phase to a visible higher amount of δ -ferrite. Fig. 10 shows many regions where δ -ferrite appears, as small darker areas. It is evident that for specimens exposed to CSI cycles in the HoSIER (Figs. 10 (SA), (SB), (SC) and (SD)) the quantity of this zones is denser in for the same picture area considered; then, with this evidence and with X-ray diffraction technique and SEM and EDXS analysis it is concluded the formation of δ -ferrite.

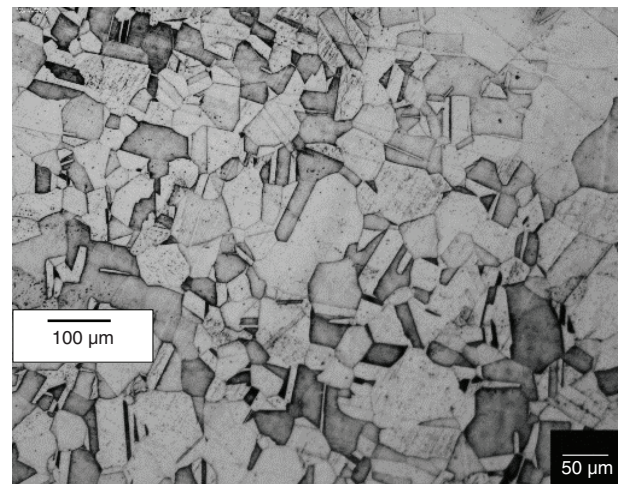


FIGURE 9. As-rolled AISI 316 stainless steel specimen, 200X.

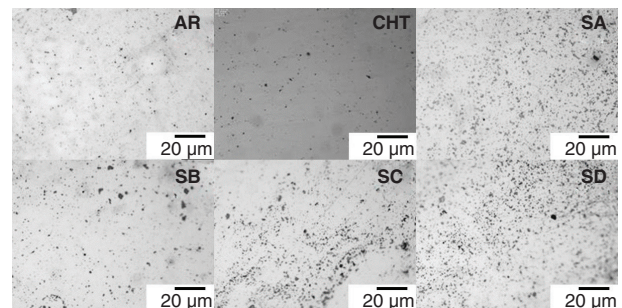


FIGURE 10. Metallographies with magnification of 500X with etchant 2 for (AR) specimen with no heat treatment and no mechanical traction test, (CHT)specimen with conventional heat treatment and no traction test, and (SA), (SB), (SC), (SD) for specimens A, B, D, and D respectively.

4. CONCLUSIONS

- A photo-thermal cycle experiment was performed on AISI 316 SS specimens using the HoSIER located in the UNAM-Conacyt in the city of Temixco, Morelos, México. The specimens proposed for this study were of the same dimensions as the cylindrical pipes used as concentrated solar irradiation elements in the receivers of central tower systems. Based on the experiments performed and the mechanical, de OM and the SEM and EDXS analysis, and X-ray diffraction studies performed after the experiments, the following conclusions can be made:
- There is no evidence of relevant changes in the tensile mechanical properties due to the number of photo-thermal cycles applied to the specimens. Thus, degradation caused by photo-thermal fatigue does not occur if the number of cycles is low compared to the lifetime and the number of cycles in the operational lifetime of a solar central tower receiver. This tensile mechanical properties are not affected by the appearance of δ -ferrite either, if low cycle number is performed. For other mechanical conditions of applied stress, it will be necessary to carry out the corresponding tests.
- A developed phase identified as crystalline δ -ferrite, is formed in the matrix of AISI 316 SS. The phase was found to be present by OM analysis and X-ray diffraction technique and as constitutive elements Fe and Cr were confirmed by EDXS analysis. High Fe atomic percentage content over the surface with respect to CHT specimen gives a first idea of the δ -ferrite dispersed phase.
- The dispersed δ -ferrite crystalline phase is present in the specimens treated with CSI -in which the UV fraction of the solar spectrum has influence-, and the temperature obtained at the time; however, this phase does not appear in the same material when no treatment is conducted or when it is treated by conventional heat treatments at a similar mean temperature. Hence, the CSI denotes the possibility of modifying the crystalline phases of AISI 316 SS at temperatures near 630 °C, allowing us to suggest that the UV fraction of the solar spectrum has an influence as an allotropy activator. At the higher temperatures for the experiments carried out, the oxidation showed an inhibited behavior; giving rise to a particular situation where a more feasible oxidation would be expected.
- Further investigation as an electrochemical corrosion test is suggested be performed to determine if the new phase formed in the original AISI 316 SS matrix has an effect on the corrosion behavior of these materials.

ACKNOWLEDGEMENTS

The authors thank the PAPIIT projects (IN115416) and PAPIIT (IT101318) “Desarrollo de Tecnologías de Superficies para la Optimización de Componentes y Sistemas” DGAPA, and UNAM for their support. The authors thank Eliezer Hernández Mecinas in Laboratorio de Pruebas Mecánicas IIM-UNAM, María L. Ramón García in Departamento de Materiales Solares IER-UNAM, Jorge Luis Romero Hernández in DIMEI, Facultad de Ingeniería, UNAM, and José Campos Álvarez in Departamento de Materiales Solares IER-UNAM for their support.

REFERENCES

- Augsburger, G., Favrat, D. (2013). Modelling of the receiver transient flux distribution due to cloud passages on a solar tower thermal power plant. *Sol. Energy* 87, 42–52. <https://doi.org/10.1016/j.solener.2012.10.010>.
- Bechtoldt, C.J., Vacher, H.C. (1957). Phase-Diagram Study of Alloys in the Iron-Chromium-Molybdenum-Nickel System. *J. Res. Nat. Bur. Stand.* 58 (1), 7–19. <https://doi.org/10.6028/jres.058.002>.
- Boerema, N., Morrison, G., Taylor, R., Rosengarten, G. (2012). Liquid sodium versus Hitec as a heat transfer fluid in solar central receiver systems. *Sol. Energy* 86 (9), 2293–2305. <https://doi.org/10.1016/j.solener.2012.05.001>.
- Boubault, A., Claudet, B., Faugoux, O., Olalde, G., Serra, J. (2012). A numerical thermal approach to study the accelerated aging of a solar absorber material. *Sol. Energy* 86 (11), 3153–3167. <https://doi.org/10.1016/j.solener.2012.08.007>.
- Boubault, A., Claudet, B., Faugoux, O., Olalde, G. (2014). Aging of solar absorber materials under highly concentrated solar fluxes. *Sol. Energ. Mat. Sol. C.* 123, 211–219. <https://doi.org/10.1016/j.solmat.2014.01.010>.
- Brooks, J.A., Baskes, M.I., Greulich, F.A. (1991). Solidification modeling and solid-state transformations in high-energy density stainless steel welds. *Metall. Trans. A* 22 (4), 915–926. <https://doi.org/10.1007/BF02659001>.
- Dieter, G.E. (1986). *Mechanical behavior under tensile and compressive loads*. ASM Handbook, Vol. 8, pp. 99–108.
- EI Nayal, G., Beech, J. (1986). Relationship between composition, impurity content, cooling rate, and solidification in austenitic stainless steels. *Mater. Sci. Technol.* 2 (6), 603–610. <https://doi.org/10.1179/mst.1986.2.6.603>.
- Fine, M.E., Chung, Y. (1996). *ASM Handbook, Vol. 19, Fatigue and Fracture*. ASM International, USA, pp. 148–149.
- Herranz, G., Rodríguez, G.P. (2010). *Uses of Concentrated Solar Energy in Materials Science. In Solar Energy*. Edited by R. Rugeescu, IntechOpen, p. 432. <https://doi.org/10.5772/8067>.
- Hsieh, C.C., Lin, D.Y., Chen, M.C., Wu, W. (2008). Precipitation and strengthening behavior of massive δ -ferrite in dissimilar stainless steels during massive phase transformation. *Mat. Sci. Eng. A-Struct.* 477 (1–2), 328–333. <https://doi.org/10.1016/j.msea.2007.05.037>.
- Ho, C.K., Iverson, B.D. (2014). Review of high-temperature central receiver designs for concentrating solar power. *Renew. Sustain. Energy Rev.* 29, 835–846. <https://doi.org/10.1016/j.rser.2013.08.099>.
- Jianfeng, L., Jing, D., Jianping, Y. (2010). Heat transfer performance of an external receiver pipe under unilateral concentrated solar radiation. *Sol. Energy* 84 (11), 1879–1887. <https://doi.org/10.1016/j.solener.2009.11.015>.
- Klobčar, D., Tušek, J., Taljat, B. (2008). Thermal fatigue of materials for die-casting tooling. *Mat. Sci. Eng. A-Struct.* 472 (1–2), 198–207. <https://doi.org/10.1016/j.msea.2007.03.025>.
- Padilha, A.F., Tavares, C.F., Martorano M.A. (2013). Delta Ferrite Formation in Austenitic Stainless Steel Castings.

- Mater. Sci. Forum* 730–732, 733–738. <https://doi.org/10.4028/www.scientific.net/MSF.730-732.733>.
- Prasad, K., Kumar, V. (2013). Temperature gradients in flat thermomechanical fatigue specimens. *Appl. Therm. Eng.* 59 (1–2), 131–133. <https://doi.org/10.1016/j.applthermaleng.2013.05.002>.
- Riveros-Rosas, D., Herrera-Vázquez, J., Pérez-Rábago, C.A., Arancibia-Bulnes, C.A., Vázquez-Montiel, S., Sánchez-González, M., Granados-Agustín, F., Jaramillo, O.A., Estrada, C.A. (2010). Optical design of a high radiative flux solar furnace for Mexico. *Sol. Energy* 84 (5), 792–800. <https://doi.org/10.1016/j.solener.2010.02.002>.
- Rodríguez-Sánchez, M.R., Soria-Verdugo, A., Almendros-Ibáñez, J.A., Acosta-Iborra, A., Santana, D. (2014). Thermal design guidelines of solar power towers. *Appl. Therm. Eng.* 63 (1), 428–438. <https://doi.org/10.1016/j.applthermaleng.2013.11.014>.
- Rojas-Morín, A., Fernández-Reche, J. (2011). Estimate of thermal fatigue lifetime for the INCONEL 625LCF plate while exposed to concentrated solar radiation. *Rev. Metal.* 47 (2), 112–125. <https://doi.org/10.3989/revmetalmadrid.1038>.
- Sibin, K.P., Siju, J., Harish, C.B. (2015). Control of thermal emittance of stainless steel using sputtered tungsten thin films for solar thermal power applications. *Sol. Energ. Mat. Sol. C.* 133, 1–7. <https://doi.org/10.1016/j.solmat.2014.11.002>.
- Saeidi, K., Gao, X., Lofaj, F., Kvetková, L., Shen, Z.J. (2015). Transformation of austenite to duplex austenite-ferrite assembly in annealed stainless steel 316L consolidated by laser melting. *J. Alloy. Compd.* 633, 463–469. <https://doi.org/10.1016/j.jallcom.2015.01.249>.
- Sokolov, S., Ortel, E., Radnik, J., Kraehnert, R. (2009). Influence of steel composition and pre-treatment conditions on morphology and microstructure of TiO₂ mesoporous layers produced by dip coating on steel substrates. *Thin Solid Films* 518 (1), 27–35. <https://doi.org/10.1016/j.tsf.2009.06.009>.
- Vacher, H.C., Bechtoldt, C.J. (1954). Delta Ferrite-Austenite Reactions and the Formation of Carbide, Sigma, and Chi Phases in 18 Chromium-8 Nickel-3.5 Molybdenum Steels. *J. Res. Nat. Bur. Stand.* 53 (2), 67–76. <https://doi.org/10.6028/jres.053.008>.
- Vander Voort, G.F. (1999). *Metallography Principles and Practice*. ASM International, USA.
- Yajiang, L.I., Juan, W., Bing, Z., Tao, F. (2002). XRD and TEM analysis of microstructure in the welding zone of 9Cr-1Mo-V-Nb heat-resisting steel. *B. Mater. Sci.* 25 (3), 213–217. <https://doi.org/10.1007/BF02711156>.
- Zhang, Q., Li, X., Chang, Ch., Wang, Z., Liu, H. (2013). An experimental study: Thermal performance of molten salt cavity Receivers. *Appl. Therm. Eng.* 50 (1), 334–341. <https://doi.org/10.1016/j.applthermaleng.2012.07.028>.